PCCP

Adjusting the Balance between Hydrogen and Chalcogen Bonds

Journal:	*Physical Chemistry Chemical Physics*
Manuscript ID	CP-ART-10-2022-004591.R1
Article Type:	Paper
Date Submitted by the Author:	16-Nov-2022
Complete List of Authors:	Scheiner, Steve; Utah State University, Department of Chemistry and Biochemistry

Adjusting the Balance between Hydrogen and Chalcogen Bonds

Steve Scheiner*
Department of Chemistry and Biochemistry
Utah State University
Logan, Utah 84322-0300

email: steve.scheiner@usu.edu

Abstract

A complex is assembled which pairs a carboxyl group of X_1COOH with a 1,2,5-chalcogenadiazole ring containing substituents on its C atoms. The OH of the carboxyl group donates a proton to a N atom of the ring to form a OH··N H-bond (HB), while its carbonyl O engages in a Y··O chalcogen bond (ChB) with the ring in which Y=S,Se,Te. The ChB is strengthened by enlarging the size of the Y atom from S to Se to Te. Placement of an electron-withdrawing group (EWG) X_1 on the acid strengthens the HB while weakening the ChB; the reverse occurs when EWGs are placed on the ring. By selection of the proper substituents on the two units, it is possible to achieve a near perfect balance between the strengths of these two bonds. These bond strengths are also reflected in the NMR spectroscopic properties of the chemical shielding of the various atoms and the coupling between the nuclei directly involved in each bond.

keywords: cooperativity; AIM; NBO; NMR; electrostatic potential

INTRODUCTION

A great deal has been learned about the origins and properties of the venerable H-bond (HB) over its century of study [1-7]. Its stability is based on several factors, one of which is an electrostatic attraction between a positively charged H and a nucleophile which bears an opposite charge. A second factor arises from a stabilizing transfer of charge from the base to a σ*(AH) antibonding orbital of the A-H proton-donating unit. This transfer is partly responsible for the characteristic weakening of the covalent A-H bond, and the associated red shift of its A-H stretching frequency. There is also an accompanying downfield shift of the bridging proton's NMR signal arising from a displacement of electron density as the proton donor is polarized by the field of the nucleophile. A solid base of knowledge has accumulated concerning how an electric charge or substituents on either the proton-donating or accepting unit affect the strength of the HB.

Recent years have witnessed a rapidly growing interest and study of noncovalent interactions that are closely related to the HB, in which the bridging H is replaced by any of a long list of other atoms. These noncovalent bonds are commonly categorized by the column of the periodic table from which this substitute bridging atom is derived. The halogen bond, for example, occurs when it is Cl, Br, or I in this position [8-16], with analogous designations for pnicogen and tetrel bonds as other classifications [17-25]. (First-row atoms like F and N rarely participate in these bonds [26, 27].) The chief difference with HBs is that unlike the bridging H which is characterized by an overall partial positive charge, the electrostatic potential surrounding the replacement nucleus is more anisotropic and nuanced. Although this atom can be negatively charged overall, there are one or more spatially restricted positive regions, commonly referred to as σ-holes.

Of this group of noncovalent bonds, the chalcogen bond (ChB), containing S, Se, or Te, presents a particularly interesting and wide-ranging set of properties and applications. It is prominent in catalysis [28-31], for example by activating alkenes [32], catalysis by sulfonium salts [33], or as a transfer hydrogenation catalyst [34]. Its function extends to biological systems as for example in enzyme activity of glutathione peroxidase [35] or glutathione peroxidase [35] or as an important element in SAM riboswitches [36]. The ChB is involved in other diverse applications [37], as for example enantioseparation in liquid-phase chromatography [38], assembly of porous low-density organic frameworks [39] or dimeric capsules [40], or chiral self-sorting of homochiral double helicates [41]. An intramolecular ChB influences cis/trans isomerization involved in photoswitching [42]. An interested reader is referred to several quality reviews of this phenomenon [43-48], including their participation in biological phenomena[49-52] such as proteins and nucleic acids.

These bonds run a wide gamut of strength [53], some of which are considerably stronger than a HB. They can accommodate various sorts of electron donors besides the usual bases, even including metal atoms, for example the d_z2 orbital of planar Pd, Pt [54, 55] or even W [56]. A particularly interesting facet of ChBs derives from the typical divalent bonding of the central atom which leads to the presence of two separate and distinct σ-holes, each of which can participate in a ChB with a nucleophile. A second aspect is the presence of two lone pairs on

each atom, each of which can act as an electron donor. Consequently, chalcogen atoms can bind to one another, forming triangular, square, or even larger Ch_n arrangements [57-62].

Chalcogenadiazoles hold a special place in the study of ChBs. This sort of molecule places a Ch atom between two N atoms in the context of an aromatic 5-membered ring. As such, the adjacent Ch and N atoms can act respectively as electron acceptor and donor with one or more other molecules. This quality has earned this unit a great deal of study in recent years. Cozzolino et al [63] showed they have a distinct tendency to establish intermolecular links in the solid state through secondary bonding interactions, while Ishigaki et al [64] focused on the competition between a ChB and a XB in determining crystal structure or as synthon to form a clathrate [65]. The interaction of this unit with several anions was investigated quite recently [66]. These species have found application in solid-state assembly [65] by virtue of the two σ-holes on each Ch atom. The $(ChN)_2$ square bonding motif of chalcogenadazole dimers that contains a pair of ChBs was the subject of recent quantum chemical analyses and the various geometric dispositions in which two related molecules can pair up was probed as well [67]. The placement of halogen atoms on chalcogenadiazoles enable elucidation of the factors involved in the competition between a XB and ChB [59]. The strength of the HB was also thrown into the mix with the other two [68] for a series of 1,3,4-chalcogenadiazoles. The authors noted that by enlarging either the X or Ch atom, the corresponding XB and ChB can occur at the expense of the HB. Navarro-García et al [69] showed how the ChB and HB can combine with one another in binding of halides.

Indeed, the competitive strengths of the HB and ChB in which a chalcogenadiazole can participate is of especial interest [70]. Both sorts of bonds are present in a number of crystals [71] that contain a Ch_3 triangular motif, generally both to the same Ch atom. HBs combine with ChBs when the carboxyl acid group located on a phenyl ring engages in a cocrystal with benzoselenenadiazole [72]. A similar sort of motif also occurs [73] wherein both the Se and N atom are located on a selenadiazole where the electron donor to the ChB is a N-oxide, and the proton donor is a CH group.

The prior work has opened the window to an interesting and important question concerning the competition that might exist between the HB and ChB, both of which the chalcogenadiazole is capable of. Its Ch atom is empowered to engage in a ChB via its two N neighbors on the ring, each of which imparts a substantial σ-hole on Ch. These N atoms each contain a lone pair that is coplanar with the aromatic ring which can be used to engage with a proton donor. The general system pairing 1,2,5-chalcogenadiazole derivatives with a carboxylic acid which can be used to probe this question is pictured in Fig 1 where Y refers to the Ch atom on the ring. The carboxyl group contains the seeds of both the HB and ChB: the carbonyl O can donate density to the Y σ-hole while its OH serves as proton donor to N_2 of the ring. The relative strengths of the two bonds can be manipulated in a number of ways. The size of the Y atom is known to have a strong effect on the ChB strength so S, Se, and Te are each applied in turn for Y. The X_1, X_3, and X_4 substituents on the two units were each varied from the electron-releasing NH_2 and CH_3

to electron-withdrawing NO_2 and CN. In addition, the effect of a full positive charge on the ring was tested by adding a proton to the N_2 atom.

The working hypothesis here is that the placement of an electron-withdrawing group (EWG) X_1 on the carboxyl unit ought to intensify the positive charge on its H, thereby strengthening the HB. This same EWG should weaken the ChB by reducing the availability of the carbonyl O lone pair. In a parallel vein, EWGs on the ring can be expected to strengthen the ChB while weakening the HB. The strengths of the two bonds should thus be capable of being finely tuned, as will the competitive balance between them. It is these ideas which are tested here by quantum calculations. Of particular interest is the precise combination of three substituents which afford a balance between the two bonds. Another issue to be addressed is the other extreme: how far out of balance can one get with other choices of substituents. Of interest as well is the degree to which the identify of the chalcogen atom affects this balance.

METHODS

The Gaussian 16 [74] suite of programs was employed for quantum chemical calculations. Density functional theory (DFT) employed the M06-2X functional [75], in the context of the aug-cc-pVDZ basis set which includes both polarization and diffuse functions added to a double-ζ foundation. Numerous past calculations of related systems have confirmed the dependability and accuracy of this combined approach [15, 58, 67, 71, 76-82]. The aug-cc-pVDZ-PP pseudopotential [83] was applied to fourth-row Te as it takes into account certain relativistic effects. The larger triple-ζ aug-cc-pVTZ set was used to compute specialized electronic parameters, such as charge transfers, NBO, and AIM properties, along with the all-electron cc-pVTZ-DK3 basis for Te. The computation of NMR spectral data also used aug-cc-pVTZ, but applied the NMR-DKH(TZ2P) basis for Te which was designed with NMR properties in mind. These basis sets were extracted from the EMSL Basis Set Exchange [84].

The geometries of monomers and complexes were optimized with no symmetry constraints, and were verified as true minima by normal mode analysis. Each interaction energy E_{int} is defined as the difference between the energy of the dyad and the sum of the energies of the two monomers in the geometry they adopt within the dimer. Basis set superposition error was then removed from E_{int} by the standard counterpoise protocol [85]. A recent investigation [86] concluded that combining this correction with a double-ζ basis like aug-cc-pVDZ provides results in excellent agreement with complete basis set calculations within a DFT framework. Bond paths, and the density at their bond critical points, were elucidated by the QTAIM method [87-89] by the use of the AIMAll program [90]. The NBO method [91, 92] as incorporated in Gaussian, was applied to quantify interorbital charge transfers and their energetic manifestation. The Multiwfn program [93] located the extrema of the molecular electrostatic potential (MEP) on the ρ=0.001 au isodensity surface of each monomer.

RESULTS

The fundamental 1,2,5-chalcogenadiazole system under study is exhibited in Fig 1, where X_1, X_3, and X_4 refer to various substituents, and Y indicates the particular chalcogen atom in the ring. The two principal noncovalent bonds within the complex with carboxylic acids are the $OH\cdot\cdot N_2$ H-bond, and the $Y\cdot\cdot O_2$ chalcogen bond, characterized respectively by the two R distances labeled in Fig 1.

Energetics

The total interaction energy of each fully optimized complex E_{int} is displayed in the fourth column of Table 1 where several patterns are in evidence. These quantities as a group rise along with the size of the Y chalcogen atom S < Se < Te. Within any particular subgroup with a fixed Y, the interaction energy rises in the order X_1 = Me < H < NH_2 < CN < NO_2. With respect to substituents on the ring X_3 and X_4, a pair of cyano groups yields the smallest interaction energy, followed by two amino groups, and then a single nitro. This pattern is altered with the largest chalcogen atom Te, where it is the NO_2 group that is associated with the smallest interaction energy. Placing a charged group on the ring, whether positive or negative, raises this interaction energy.

It is of some interest to compare the relative contributions of the HB and ChB to the total interaction energy. One means of estimating these quantities is to recalculate the interaction energy following 90° rotations of one unit relative to the other. A rotation of this sort around the $H\cdot\cdot N_2$ axis leaves the HB intact while breaking the ChB, whereas a similar rotation around the $O_2\cdot\cdot Y$ axis preserves the ChB. The resulting interaction energies are listed in the next two columns of Table 1 as E_{HB} and E_{ChB}, where they may be compared with one another.

Considering the S set first, growing electron-withdrawing capacity of X_1 enhances the HB from 5.5 kcal/mol for Me up to 11.5 kcal/mol for NO_2. This same trend persists for Y=Se and Te, although the HB becomes marginally stronger as Y grows larger. Placement of a pair of NH_2 groups on the ring slightly enhances the HB but the reverse effect of a weakening HB occurs for the electron-withdrawing NO_2 and CN substituents X_3 and X_4. These trends are understandable on the basis of the ability of electron-withdrawing groups on the acid to strengthen the HB, while pulling density from the lone pair of the base would have an opposite effect. The roles of the two subunits are reversed in the ChB, in that the COOH acts as electron donor and Y of the ring is the acceptor. It is therefore understandable that the ChB grows in strength as X_3 and X_4 sites are occupied by NO_2 or CN. Placing a full positive charge on the ring provides an even bigger boost to the ChB strength as it better enables Y to accept density. Conversely, a negatively charged substituent on the ring, which amplifies the ability of the ring N_2 to donate charge, really exaggerates the HB. The particular substituent X_1 has much less of an effect.

On a quantitative level, there is an overall growth in the HB strength as Y becomes larger. This trend can be understood as larger Y atoms are less electronegative, and thus less able to withdraw density from the adjacent N lone pair which is used in the HB. At the same time, one sees also that the larger Y atoms lead to a substantial strengthening of the ChB, in line with many other studies which attribute this tendency to a more electropositive and polarizable Y.

Of particular interest is the manner in which these principles affect the relative strengths of the two bonds. Considering Y=S first, in most cases the HB is considerably stronger than the ChB, with the exceptions at the bottom of the table for the dicyano substituted ring and the cationic rings. The same trend is true for Se, for which the nitro-substituted ring also contains a stronger ChB than HB. There is a continuation of this shift for the larger Te where the ChB grows in strength relative to the HB and even becomes equivalent for NH_2/H/H substituents.

A convenient and compact means of comparing the strengths of the two bonds is via their ratio, which is reported in the next column of Table 1. As can be seen there, the ChB/HB ratio amounts to only some 0.24-0.40 for most of the S complexes. It grows a bit for X_3=NO_2, and then exceeds unity for the dicyano-substituted ring, and especially for the cations. This ratio is somewhat larger for Y=Se, particularly for the protonated ring where the HB energy is less than 1 kcal/mol. The growth in E_{ChB}/E_{HB} continues further for Te. It remains below unity for the majority of complexes but the ChB clearly exceeds the HB by a healthy margin when electron-withdrawing NO_2 or CN are placed on the ring, or if it is imbued with a positive charge.

Since the two bond types involve charge transfer in opposite directions, one would expect them to reinforce one another. This amplification can be quantified by the difference between the total interaction energy within the complex and the sum of the HB and ChB energies, each computed in the absence of the other. This cooperativity (coop) is presented in the penultimate column of Table 1 where it can be seen to be quite substantial. While quite small in several cases, less than 5% of the total interaction energy, it is much larger, up to nearly 30% in other complexes.

With charge transfer within the HB passing from the ring to the carboxyl, while it moves in the reverse direction within the ChB, the direction of net transfer can offer another clue as to the competitive strengths of these two bonds. The total charge on the carboxyl-containing molecule is contained in the last column of Table 1 as CT, where a negative sign indicates net accumulation of density on this unit, i.e. the HB transfers more charge than does the ChB. This quantity is in fact most negative for the smallest E_{ChB}/E_{HB} ratios, as would be expected. It attains a positive value near the bottom of each section of Table 1 where the ratio exceeds unity and the ChB is stronger than the HB. And as the Y atom grows larger, and with it a stronger ChB, the value of CT becomes less negative/more positive for any given set of substituents, particularly so for Te.

Geometrical Properties

The geometrical aspects of these complexes provide further clues into the strengths of these bonds. In the first place, it is generally accepted that a stronger bond will draw the two subunits in closer to one another. In the particular case of HBs of the OH··N type, there is also a tendency for a stronger intermolecular interaction to elongate the covalent OH bond. The fourth and fifth columns of Table 2 allow comparisons to be made concerning both the HB and ChB length. Due to the small radius of a H atom, the HB lengths are of course considerably shorter than R_{ChB}. What is of greatest interest are the trends in these two quantities as the substituents or Y atoms

are altered. For any Y atom, replacement of the X_1 substituent on the acid unit by an EWG shortens the HB, whereas these same substituents lengthen this bond when placed on the ring. This pattern confirms the energetic E_{HB} quantities in Table 1. An opposite trend characterizes the ChB length, again consistent with energetic patterns. These ideas are more explicit in the next two columns of Table 2 which describe how each length compares with that in which there are no substituents, i.e. X_1=X_3=X_4=H. In the majority of cases, it is the HB length which is a bit more sensitive to substituent than is the ChB distance. The clear exception arises when the ring acquires a positive charge which greatly ramps up the ChB strength, with a smaller weakening of the HB.

The next two columns of Table 2 contain the changes within the two most relevant internal bondlengths that arise when the two subunits are allowed to interact with one another. The stretches within the OH bond of the acid Δr(OH) are consistent with the forgoing data. These elongations are largest when X_1 represents an EWG, but diminish when these same substituents are placed on the ring.

In contrast, the changes within the Y-N_5 bond within the ring are more complicated, suffering a contraction in most, but not all cases. This behavior arises as the result of two conflicting tendencies, a different one arising from each sort of bond. The transfer of electron density into the $\sigma^*(YN_5)$ antibonding orbital in the context of a ChB would tend to lengthen this bond. Indeed, partial optimization of the unsubstituted X_1=X_3=X_4=H complex, with Y=Se, with the H-bond broken by a 90° rotation around the O··Se axis, elongates this bond by some 0.003 Å. On the other hand, if the ChB is broken by a 90° rotation that leaves the HB intact, this same YN_5 bond is contracted by a larger amount of 0.007 Å. As a net result, a strengthening HB will tend to shorten this bond while it will be elongated if the ChB is magnified. So one can see that as the X_3 and X_4 substituents become more electron-withdrawing, the contracting effects of the HB are attenuated, and the net result can become elongating for the strongest ChB combined with the weaker HB near the bottom of each segment of Table 2.

Along with the modulation of the HB and ChB lengths comes a small reorientation of the two molecules relative to one another. As the HB weakens, there is also a tendency for the HB to become less linear. So taking the Se systems as illustrative, the tenth column of Table 2 shows that the $\theta(O_1H\cdot\cdot N_2)$ angle drops from 170° for the systems with X_1=CN or NO_2 with their strong HB, down to 155° for the protonated complex. This same weakening of the HB also strengthens the ChB, which tends to make the $N_5Y\cdot\cdot O_2$ alignment more linear, although this angle is less sensitive to bond strength, as is evident in the penultimate column of Table 2.

Like their strengths, the lengths of the HB and ChB tend to vary in opposite directions, i.e. one elongates while the other contracts. So one might expect the overall distance between the two subunits to be fairly insensitive to substitution patterns. The final column of Table 2 lists this intermolecular distance R_{inter} measured between the carboxyl C and the geometric center of each ring. This quantity is fairly constant, lying in the range between 4.15 and 4.41 Å but does display certain subtle trends nonetheless. For any subgroup with a particular chalcogen Y atom, the cationic system has the shortest intermolecular distance. As X_1 becomes more electron-

withdrawing and the HB shortens, so does R_{inter}, but this distance is less affected by the identity of X_3 and X_4. The distance between the two molecules consistently shortens, albeit by only a little, as Y grows larger, reflecting the growing ChB strength.

Electronic Properties

A. Charge Transfer

There are a number of other markers of the strengths of the two noncovalent bonds arising from analysis of each wavefunction. For both a HB and ChB there is a certain amount of charge transfer between the two units. In the case of the HB in Fig 1, charge will be transferred from the N_2 lone pair to the σ*(OH) antibonding orbital; it is the O_2 lone pair that transmits charge to the σ*(YN_5) orbital. The amount of this charge is quantified by E(2), the NBO second-order perturbation energy to which it corresponds. These quantities are contained in the fourth and fifth columns of Table 3. It is problematic to compare the values of E(2) for two different sorts of bonds, HB and ChB to one another, but it is certainly valid to examine the patterns arising for each bond from changes in Y or substituent.

The HB E(2) values conform nicely to the energetic and geometrical parameters discussed above. For Y=S, for example, E(2) is roughly 20 kcal/mol for the first three rows, but rises as the electron-withdrawing CN and NO_2 groups are placed on the X_1COOH molecule or if the ring acquires an overall negative charge. Conversely, these same groups lower E(2) when placed on the aromatic ring. As Y grows larger, E(2) is magnified but the trends remain. The ChB Y··O E(2) quantities are in most cases smaller than those for the HBs, and the effects of the X_1, X_3, and X_4 substituents are reversed, as is true for the energetic and geometric markers. Again the larger Y atoms lead to stronger ChBs, and their attendant growing E(2). Note the particularly large ChB charge transfer parameter within the ionic system where a cationic ring is paired with HCOOH.

B. Electron Density Topology

Analysis of the electron density of each complex via the AIM protocol provides bond paths for both the HB and ChB. The density of the bond critical point roughly midway between the two nuclei ρ_{BCP} offers an alternate means of estimating the strength of each bond. These quantities listed in the next two columns of Table 3 again fall into the patterns evinced by the previous parameters. The HB is strengthened by EWGs on the carboxyl-containing unit while an enhancement of the ChB occurs when they are placed on the ring or if the ring acquires a positive charge. In either case, the changes are reciprocal in that HB weakening is accompanied by enhancement of the ChB. There is also the familiar pattern that both sorts of bonds are strengthened by a larger Y: S < Se < Te. In terms of a quantitative comparison, ρ_{BCP} is uniformly larger for the HB than for the ChB; the exceptions occur for the cationic ring. This finding is generally consistent with the energies computed for the individual bond strengths in Table 1.

C. NMR Spectra

Bond strengths can be assessed from a very different angle by evaluating the NMR coupling constants between the relevant atoms that interact directly with one another. The greatly differing magnitudes of the gyromagnetic ratios of the various nuclei can be factored out by considering the reduced coupling constant K which is related to J by

$$K = 4\pi^2 J/h\gamma_A\gamma_B \quad (1)$$

where γ refers to the gyromagnetic ratios of the two relevant nuclei. The calculated values of K are displayed in the last two columns of Table 3 where it may first be noticed that the HB K is generally negative and small in magnitude, while that for the ChB is consistently positive and much larger in magnitude. This distinction should not be construed as suggesting that the HBs are much weaker than the ChBs, but simply an outgrowth of the different nature of the participating nuclei.

The behavior of these coupling constants is only poorly correlated with the other parameters discussed above. The strengthening of each HB with EWG on the carboxyl group is correlated with a drop in the magnitude of K; nor is there much sensitivity of K(H··O) to substituents on the ring. The coupling constant fails to capture the growth in HB strength as Y grows in size. On the other hand, K(Y··O) properly reflects the weakening of the ChB when EWGs are placed on the acid species, and this quantity rises along with growing ChB strength when EWGs are added to the ring (although the latter trend is not in evidence for Te). Moreover, the ChB K consistently reflects the stronger ChB for larger Y atoms.

Also of great utility in analysis of noncovalently bonded complexes is the change in the NMR chemical shift of the nuclei participating in these bonds. Table 4 reports the change in chemical shielding of the nuclei involved in both the HB and ChB in these complexes. The loss of shielding around the H-bonding proton corresponds to its well documented downfield shift. As is typically the case, the amount of this shift is closely related to the strength of the HB, as measured by the energetic quantities in Table 1 or any of the electronic parameters in the succeeding tables. The hydroxyl O_1 to which this proton is bound also suffers a loss of shielding, which is roughly proportional to the HB strength. In fact, this O atom is even more sensitive to HB strength than is the bridging H. The exception to this rule is the large O_1 shielding drop for the cationic systems, despite their weak HB. The N_2 atom which donates density to the HB undergoes a large increase in its chemical shielding. However, the magnitude of this rise is poorly correlated with HB strength, particularly within the subset where substituents are added to the ring.

The carbonyl O_2 atom of the X_1COOH unit acts as electron donor to the Y of the ring in the ChB. The shielding of this nucleus rises upon complexation, and the magnitude of this increase rises quickly as X_1 becomes more electron-withdrawing, much more so than the ChB energy of Table 1 or of any of the other YB strength indicators discussed above. In fact, this rise contrasts with the slight weakening of the ChB. The increase in the O_2 chemical shielding is most dramatic as EWGs are placed on the ring, even tripling as the ring acquires a positive charge. Unlike O_2, the Y atom suffers a small diminution of its shielding for Y=S, but is increased by a

large amount for Y=Te; changes are small and of either sign for Se. There is a complicated pattern relating the Y shielding change to the ChB strength, which depends upon the identity of the Y atom.

D. Electrostatic Potentials

A last useful quantity is more predictive than an actual measure of noncovalent bond strength. This parameter is based on the idea that a primary factor in the formation of a noncovalent bond is the electrostatic attraction between the positive region of the molecular electrostatic potential (MEP) surrounding the Lewis acid and a negative area on its counterpart. This surface is illustrated in Fig 2 for the unsubstituted selenadiazole and MeCOOH units as examples, where blue and red colors respectively indicate positive and negative regions. One of the two Se σ-holes is plainly visible in Fig 2a, as is the red lone pair region of the N center. The positive carboxyl H is reflected by its surrounding blue area, as is the negative segment near the carbonyl O in Fig 2b.

The entire positive area is frequently encapsulated as the potential of a single point, that of the maximum of the MEP on an isodensity surface, and the negative region of the base as the MEP minimum on an analogous surface. In the case of a complex like those contained here, where there are two noncovalent bonds, there are two extrema of concern on each subunit. Taking X_1COOH as an example, the maximum around the proton is of interest as is the minimum on the carbonyl O which interacts with the Y of the ring. The maximum and minimum of interest on each ring is likewise that on the Y atom, and that on the N_2, respectively.

These extrema are reported in Table 5 and display predictable properties. Electron-releasing NH_2 and Me reduce the maximum on the proton of X_1COOH, while the EWGs yield the opposite effect. The minimum on the carbonyl O is affected in the opposite manner in the sense that the minimum grows larger/smaller with an electron-releasing/withdrawing substituent. It might be noted from the first rows of Table 5 that the substituent effect is somewhat more perturbing for the H maximum than for the O minimum. The next rows contain comparable information for the various rings. Again, an EWG enhances the maximum on Y, while reducing the minimum on N; opposite patterns characterize electron-releasing amino groups as well as O^-. As for the acid unit, the effects of substituents are larger for the MEP maximum than for the minimum. The imposition of a positive charge on the ring imparts a particularly large positive increment, even making the minima positive in sign.

In quantitative terms, the values of these extrema are only mildly correlated with the energetics. For example, the product of the maximum on H of the acid and the minimum on N of the ring bears only an approximate relation to the HB energy listed in Table 1. The R^2 correlation coefficient between these two quantities is 0.63. The ChBs are less connected to the electrostatic parameters, with a correlation coefficient of 0.48 between E_{ChB} and the relevant max*min product. The inability of the MEP extrema to provide an accurate approximation of the interaction energies is not surprising. In the first place, the numerical value of the MEP at a single point, the extremum, cannot accurately capture the full electrostatic interactions between

the two subunits. Secondly, each noncovalent bond is heavily dependent on factors other than Coulombic forces, such as charge transfer and dispersion.

E. Correlations with Energetics

Quite a number of parameters appear to have certain relationships with the energy of each bond. The correlation coefficients of each parameter with the respective E_{HB} or E_{ChB} are collected in Table 6. The first two columns collect all of the data together, regardless of the nature of Y. The strongest correlations concern the HB, and specifically E(2) and ρ_{BCP}, which have R^2 of 0.99 and 0.98, respectively. The correlation is poorer for these same quantities involving the ChB with correlation coefficients of 0.89 and 0.87. The internal bond stretches in the first row of Table 6 are fairly good, with R^2~0.8. The NMR coupling constant is a poor overall determinant, as are the shielding changes of the individual atoms, with none larger than 0.8. With regard to the chemical shielding changes, the bridging H nucleus presents the closest correlation with the HB, with R^2=0.73. The ChB appears to be better correlated with the shielding of the two atoms involved, particularly 0.82 for O_2.

As a final parameter of interest, the juxtaposition of the MEP maximum of one subunit with the minimum on its partner is thought to be at least a rough indicator of the electrostatic portion of the interaction energy within a given noncovalent bond. So for example, the HB energies here might bear some relation with the product of the MEP maximum on the H of the carboxyl group and the minimum on N_2 of the ring. Likewise, the combination of the maximum located at the Y σ-hole with the minimum on O_2 might relate to the ChB strength. The last row of Table 6 considers these correlations, separately for the HB and ChB. The correlation is unimpressive, with coefficients hovering around 0.5-0.6.

However, it must be remembered that these quantities place all data within a common set with no distinction for the nature of the Y atom. The next columns of the table consider each Y as a separate subset of data, resulting in clear improvements, with some values of R^2 approaching unity. The most impressive correlations occur for the bond elongation ratio, E(2), and ρ_{BCP}, with the exception of the S ChB data. The correlation of coupling constant K with the ChB energetics is mediocre. R^2 varies from as low as 0.5 but rises up to 0.95 for Te HBs. The best determinant of HB strength amongst the chemical shielding parameters is the bridging proton. With the exception of Y=S, the shielding change of the Y atom bears a close relationship to the ChB energy. Finally considering the MEP product, the correlation of V_{max}*V_{min} lies in the 0.4 - 0.7 range.

F. Thermodynamic Properties

The evaluation of the various thermodynamic properties related to each dimerization reaction can offer some connections with experiment. These quantities are displayed in Table 7, all evaluated at 25 C. The reaction enthalpies tend to be slightly less exothermic than the electronic interaction energies reported in Table 1, largely because of the inclusion of vibrational energies. The entropy of each reaction is negative, as is common for a dimerization where two

independent molecules are blended into a single complex. ΔS is fairly uniform for all systems, on the order of -35 cal/mol K. The combination of ΔS with the enthalpies lead to the free energies of complexation in the final column of Table 7. These quantities are much less negative than ΔH, some positive and some negative. The most exothermic reactions are those with the largest interaction energies, and ΔG can reach as large a negative value as -15 kcal/mol as in the case of the protonated Te ring.

DISCUSSION

The principles governing the strengths of the two bonds fall neatly into what is already known about each. The placement of a EWG on the proton-donating molecule will amplify the positive charge on the proton and thereby strengthen the ensuing HB, while an electron-donating substituent will exert an opposite effect. Likewise, the σ-hole on the Y atom of the ring will be intensified by one or more EWGs, and even more so from a positive charge placed on the ring, which will in turn ramp up the strength of the ChB. Another trend that fits previous results is the strengthening of the ChB that occurs as the Y atom is enlarged: S < Se < Te. Since charge is moving in opposite directions for the HB and ChB, i.e. each molecule serves as both electron donor and acceptor, there is a certain degree of cooperativity between them, wherein the total interaction energy is larger than the sum of the individual bond energies. This principle also fits into well understood properties of noncovalent bonding.

The calculations have established the details of the balance between the strengths and manifestations of the two bonds. In most cases, it is the HB that is the stronger of the two, and there is a net transfer of charge from the ring to the carboxyl unit, even for Te, the largest of the Y atoms considered here. But this balance is reversed when EWGs are placed on the ring that sufficiently deepen the Y σ-hole and strengthen the ChB. A cationic ring offers the combination of a particularly strong ChB and weak HB.

The magnitudes of these bond strengths are substantial. HB interaction energies range up to as much as 17 kcal/mol when O_2NCOOH is paired with an unsubstituted ring. The ChB strengths are of the same general magnitude, all at least 2 kcal/mol, but reaching up to a maximum of 23 kcal/mol when a cationic Te ring interacts with HCOOH. When these two individual bonds are combined together, the total interaction energies of these carboxyl/ring dyads range from 9 to 33 kcal/mol, placing them in the moderate to strong category. These total interaction energies reflect a significant degree of cooperativity between the two bonds. The full interaction energy exceeds the sum of the two individual bond energies by a variable amount, but this enhancement can rise to as much as 30%.

Given the variability of the HB and ChB strengths and associated bond lengths, one might anticipate these changes to give rise to a sizable reorientation of the two subunits relative to one another. These angular adjustments fit within a 10° window. For example, the $\theta(R_c\text{-}C_1X_1)$ angle remains within 10° of linearity for all complexes, where R_c refers to the geometrical center of the ring. The largest deviations from 180° occur for the cationic ring where the ChB strength far outweighs the HB. The orientation of the ring can be measured via $\theta(C_4R_c\text{-}C_1)$. This angle lies

in the 10° range between 159° and 169°; the wider angles are generally associated with a larger E_{ChB}/E_{HB} ratio. It is notable as well that neither of the two forgoing angles displays much sensitivity to the identity of the Y atom.

An earlier study had identified a tendency for an internal HB to be preferred over a ChB [94] which is generally consistent with most of the complexes examined here. A close analogy to some of the systems described above derives from a series of cocrystals [72] wherein the carboxyl group is attached to a phenyl ring in isophthalic acid, and the ring is attached to a phenyl ring in benzoselenadiazole. Calculations of these interactions yielded AIM BCP densities slightly smaller than those computed here. HB lengths in the cocrystals were closely aligned with the optimized geometries in Table 2, but Se··O ChB lengths were slightly longer. The interaction energies computed for these pairs were 9.0 kcal/mol, slightly smaller than the results for the fully optimized pairs, consistent with the somewhat longer ChBs within the crystal.

A somewhat similar pairing of a ChB and HB was considered recently [70] when the 5-membered ring of benzochalcogenadiazole was paired with a N-base to complete the Y··N ChB. Several of the partner molecules also contained a proton donor, either CH or NH. The binding energies followed the normal ChB sequence S < Se < Te. The addition of the HB adds to the total interaction energy, and surprisingly more so for CH··N than for NH··N. Overall, the combination of a ChB and HB led to interaction energies between 3.9 and 13.6 kcal/mol, somewhat smaller than those obtained for these joint ChB/HB interactions considered here, but there was no attempt made to separate the contributions of the two bonds. Partitioning of these interactions into components led to the conclusion that dispersion represented the largest component in most cases, whether S, Se, or Te.

A similar motif has been examined [73] wherein both the Se and N atom are located on a selenadiazole. The electron donor to the ChB is a N-oxide, and the proton donor is a CH group. The range of R(Se··O) ChB lengths within these crystals were within the same range as the calculated values obtained here. Molecules related to benzochalcogenadiazoles were recently examined in the context of their chalcogen bonding to halides [66]. Given the charge-assist gained from the anion, the binding energies were fairly large, between 28 and 86 kcal/mol. This charge-assistance was echoed by another work [95] for a variety of different anions, and demonstrated the importance of classical electrostatics to this bonding.

By placing halogen substituents on the phenyl ring of benzochalcogenadiazoles, Ishigaki and Suzuki [64] were able to compare the ability of these systems to engage in halogen vs chalcogen bonding. The presence of I forced the dominance of the XB for S and Se, but Cl and Br were not powerful enough to overcome the ChB formed by Te. The X and Y atoms were far enough separated on each molecule that any cooperativity was minimized.

Calabrese et al [96] very recently considered a system in which two units were bound by a CH··O HB plus I··O/F XB. In addition to the consideration here of a XB rather than a ChB, the situation is also different than the neutral pairs considered above in that the I-containing species examined by these authors was the IO_4^- anion. This charge ought to amplify the HB while weakening any XB. Nonetheless, the XB was deemed to be the stronger of the two via

comparison of AIM data. This distinction can perhaps be rationalized on the basis of the general weakness of CH as proton donor.

Regarding the calculated NMR data, experimental measurements [97] suggest that the Se isotropic chemical shift decreases as the ChB length shortens and the bond strengthens. This trend is mirrored by the calculated data which tend toward higher Se shielding for stronger ChBs.

CONCLUSIONS

The placement of electron-withdrawing or donating substituents on the two molecules containing respectively a carboxyl group and a chalcogenadiazole can fine tune the strengths of the competing HB and ChB over a wide range. An EWG on the carboxyl group heightens the positive charge on the bridging proton, as is normally the case for HBs, but has only a minimal impact on the strength of the ChB even though it reduces the magnitude of the MEP minimum on the electron-donor O_2 atom. The EWG exerts a more dramatic strengthening influence on the ChB when placed on the ring where it intensifies the σ-hole on the Y atom, while simultaneously weakening the OH··N HB. An even larger effect of this sort is associated with the placement of a full positive charge on the ring, which reduces the HB energy to only a small fraction of that associated with the ChB.

There is a fine balance between the strengths of the HB and ChB. The former is the stronger of the two in most instances, with the exception of the placement of one or more EWGs or a positive charge on the ring. This balance is reflected also in the amounts of charge transferred in the two directions. The charge migrating from the ring to the carboxyl within the context of the HB is greater than that moving from the carbonyl O to the ring as a result of ChB formation for those cases where the HB is the stronger of the two bonds. There are a host of other markers of the individual bonds that are related to their strength, including geometric, NBO, AIM, and NMR properties.

Acknowledgements

This material is based upon work supported by the National Science Foundation under Grant No. 1954310.

Conflict of Interest

The author declares no conflict of interest.

REFERENCES

1. G. C. Pimentel and A. L. McClellan, *The Hydrogen Bond*, Freeman, San Francisco, 1960.
2. P. Schuster, G. Zundel and C. Sandorfy, *The Hydrogen Bond. Recent Developments in Theory and Experiments*, North-Holland Publishing Co., Amsterdam, 1976.
3. S. Cybulski and S. Scheiner, *J. Am. Chem. Soc.*, 1987, **109**, 4199-4206.
4. G. A. Jeffrey and W. Saenger, *Hydrogen Bonding in Biological Structures*, Springer-Verlag, Berlin, 1991.

5. S. Scheiner, *J. Indian Inst. Sci.*, 2020, **100**, 61-76.
6. M. V. Vener and S. Scheiner, *J. Phys. Chem.*, 1995, **99**, 642-649.
7. S. Scheiner, D. A. Kleier and W. N. Lipscomb, *Proc. Nat. Acad. Sci., USA*, 1975, **72**, 2606-2610.
8. I. Benito, R. M. Gomila and A. Frontera, *CrystEngComm*, 2022, **24**, 4440-4446.
9. M. d. l. N. Piña, A. Frontera and A. Bauzá, *ACS Chem. Biol.*, 2020, **15**, 1942-1948.
10. I. Alkorta, J. Elguero and J. M. Oliva-Enrich, *Materials*, 2020, **13**, 2163.
11. D. J. R. Duarte, G. L. Sosa, N. M. Peruchena and I. Alkorta, *Phys. Chem. Chem. Phys.*, 2016, **18**, 7300-7309.
12. V. d. P. N. Nziko and S. Scheiner, *Phys. Chem. Chem. Phys.*, 2016, **18**, 3581-3590.
13. S. J. Grabowski, *Chem. Phys. Lett.*, 2014, **605-606**, 131-136.
14. P. Politzer, J. S. Murray and T. Clark, *Phys. Chem. Chem. Phys.*, 2021, **23**, 16458-16468.
15. S. Scheiner, *J. Phys. Chem. A*, 2022, **126**, 6443-6455.
16. S. Scheiner, *Cryst. Growth Des.*, 2022, **22**, 2692-2702.
17. S. J. Grabowski, *Struct. Chem.*, 2019, **30**, 1141-1152.
18. L. M. Azofra and S. Scheiner, *J. Chem. Phys.*, 2015, **142**, 034307.
19. J. J. Roeleveld, S. J. Lekanne Deprez, A. Verhoofstad, A. Frontera, J. I. van der Vlugt and T. J. Mooibroek, *Chem. Eur. J.*, 2020, **26**, 10126-10132.
20. S. Scheiner, *Phys. Chem. Chem. Phys.*, 2021, **23**, 5702-5717.
21. C. Trujillo, I. Alkorta, J. Elguero and G. Sánchez-Sanz, *Molecules*, 2019, **24**, 308.
22. Z. Latajka and S. Scheiner, *J. Chem. Phys.*, 1986, **84**, 341-347.
23. V. Kumar, P. Scilabra, P. Politzer, G. Terraneo, A. Daolio, F. Fernandez-Palacio, J. S. Murray and G. Resnati, *Cryst. Growth Des.*, 2021, **21**, 642-652.
24. W. Zierkiewicz, M. Michalczyk, G. Mahmoudi, I. García-Santos, A. Castiñeiras, E. Zangrando and S. Scheiner, *ChemPhysChem.*, 2022, **23**, e202200306.
25. W. Zierkiewicz, A. Grabarz, M. Michalczyk and S. Scheiner, *ChemPhysChem.*, 2021, **22**, 924-934.
26. S. Scheiner, *J. Phys. Chem. A*, 2021, **125**, 10419-10427.
27. S. Scheiner, *J. Phys. Chem. A*, 2020, **124**, 7290-7299.
28. J. Bamberger, F. Ostler and O. G. Mancheño, *ChemCatChem*, 2019, **11**, 5198-5211.
29. R. Weiss, E. Aubert, P. Peluso, S. Cossu, P. Pale and V. Mamane, *Molecules*, 2019, **24**, 4484.
30. S. Benz, A. I. Poblador-Bahamonde, N. Low-Ders and S. Matile, *Angew. Chem. Int. Ed.*, 2018, **57**, 5408-5412.
31. R. J. Fick, G. M. Kroner, B. Nepal, R. Magnani, S. Horowitz, R. L. Houtz, S. Scheiner and R. C. Trievel, *ACS Chem. Biol.*, 2016, **11**, 748-754.
32. Q. Zhang, Y.-Y. Chan, M. Zhang, Y.-Y. Yeung and Z. Ke, *Angew. Chem. Int. Ed.*, 2022, **61**, e202208009.
33. Y. Lu, Q. Liu, Z.-X. Wang and X.-Y. Chen, *Angew. Chem. Int. Ed.*, 2022, **61**, e202116071.
34. B. Zhou and F. P. Gabbaï, *Organometallics*, 2021, **40**, 2371-2374.
35. E. Y. Tupikina, *Org. Biomol. Chem.*, 2022, **20**, 5551-5557.
36. M. d. l. N. Piña, A. Frontera and A. Bauza, *ACS Chem. Biol.*, 2021, **16**, 1701-1708.
37. N. Biot and D. Bonifazi, *Coord. Chem. Rev.*, 2020, **413**, 213243.
38. P. Peluso, A. Dessì, R. Dallocchio, B. Sechi, C. Gatti, B. Chankvetadze, V. Mamane, R. Weiss, P. Pale, E. Aubert and S. Cossu, *Molecules*, 2021, **26**, 221.

39. B. J. Eckstein, L. C. Brown, B. C. Noll, M. P. Moghadasnia, G. J. Balaich and C. M. McGuirk, *J. Am. Chem. Soc.*, 2021, **143**, 20207-20215.
40. Y.-J. Zhu, Y. Gao, M.-M. Tang, J. Rebek and Y. Yu, *Chem. Commun.*, 2021, **57**, 1543-1549.
41. Y. Tian, G. Wang, Z. Ma, L. Xu and H. Wang, *Chem. Eur. J.*, 2018, **24**, 15993-15997.
42. S. Mehrparvar, Z. N. Scheller, C. Wölper and G. Haberhauer, *J. Am. Chem. Soc.*, 2021, **143**, 19856-19864.
43. K. T. Mahmudov, A. V. Gurbanov, V. A. Aliyeva, M. F. C. Guedes da Silva, G. Resnati and A. J. L. Pombeiro, *Coord. Chem. Rev.*, 2022, **464**, 214556.
44. A. Frontera and A. Bauzá, *Cryst.*, 2021, **11**, 1205.
45. P. Scilabra, G. Terraneo and G. Resnati, *Acc. Chem. Res.*, 2019, **52**, 1313-1324.
46. L. Vogel, P. Wonner and S. M. Huber, *Angew. Chem. Int. Ed.*, 2019, **58**, 1880-1891.
47. K. Selvakumar and H. B. Singh, *Chem. Sci.*, 2018, **9**, 7027-7042.
48. R. Gleiter, G. Haberhauer, D. B. Werz, F. Rominger and C. Bleiholder, *Chem. Rev.*, 2018, **118**, 2010-2041.
49. S. Jena, J. Dutta, K. D. Tulsiyan, A. K. Sahu, S. S. Choudhury and H. S. Biswal, *Chem. Soc. Rev.*, 2022, **51**, 4261-4286.
50. H. S. Biswal, A. K. Sahu, B. Galmés, A. Frontera and D. Chopra, *ChemBioChem*, 2022, **23**, e202100498.
51. O. Carugo, G. Resnati and P. Metrangolo, *ACS Chem. Biol.*, 2021, **16**, 1622-1627.
52. J. A. Fernández Riveras, A. Frontera and A. Bauzá, *Phys. Chem. Chem. Phys.*, 2021, **23**, 17656-17662.
53. D. K. Miller, I. Y. Chernyshov, Y. V. Torubaev and S. V. Rosokha, *Phys. Chem. Chem. Phys.*, 2022, **24**, 8251-8259.
54. A. V. Rozhkov, E. A. Katlenok, M. V. Zhmykhova, A. Y. Ivanov, M. L. Kuznetsov, N. A. Bokach and V. Y. Kukushkin, *J. Am. Chem. Soc.*, 2021, **143**, 15701-15710.
55. A. Frontera and A. Bauza, *Int. J. Mol. Sci.*, 2022, **23**, 4188.
56. P. R. Varadwaj, A. Varadwaj, H. M. Marques and K. Yamashita, *Int. J. Mol. Sci.*, 2022, **23**, 1263.
57. R. Weiss, E. Aubert, L. Groslambert, P. Pale and V. Mamane, *Chem. Eur. J.*, 2022, **28**, e202200395.
58. J. Liang, Y. Shi, Y. Lu, Z. Xu and H. Liu, *CrystEngComm*, 2022, **24**, 975-986.
59. V. V. Panikkattu, A. Tran, A. S. Sinha, E. W. Reinheimer, E. B. Guidez and C. B. Aakeröy, *Cryst. Growth Des.*, 2021, **21**, 7168-7178.
60. Y. Lu, W. Li, W. Yang, Z. Zhu, Z. Xu and H. Liu, *Phys. Chem. Chem. Phys.*, 2019, **21**, 21568-21576.
61. Y. Jin, X. Li, Q. Gou, G. Feng, J.-U. Grabow and W. Caminati, *Phys. Chem. Chem. Phys.*, 2019, **21**, 15656-15661.
62. M. R. Ams, N. Trapp, A. Schwab, J. V. Milić and F. Diederich, *Chem. Eur. J.*, 2019, **25**, 323-333.
63. A. F. Cozzolino, I. Vargas-Baca, S. Mansour and A. H. Mahmoudkhani, *J. Am. Chem. Soc.*, 2005, **127**, 3184-3190.
64. Y. Ishigaki, K. Shimomura, K. Asai, T. Shimajiri, T. Akutagawa, T. Fukushima and T. Suzuki, *Bull. Chem. Soc. Jpn.*, 2022, **95**, 522-531.
65. Y. Ishigaki, K. Asai, H.-P. Jacquot de Rouville, T. Shimajiri, J. Hu, V. Heitz and T. Suzuki, *ChemPlusChem*, 2022, **87**, e202200075.

66. E. A. Radiush, E. A. Pritchina, E. A. Chulanova, A. A. Dmitriev, I. Y. Bagryanskaya, A. M. Z. Slawin, J. D. Woollins, N. P. Gritsan, A. V. Zibarev and N. A. Semenov, *New J. Chem.*, 2022, **46**, 14490-14501.
67. S. Scheiner, *J. Phys. Chem. A*, 2022, **126**, 4025-4035.
68. V. De Silva, B. B. Averkiev, A. S. Sinha and C. B. Aakeröy, *Molecules*, 2021, **26**, 4125.
69. E. Navarro-García, B. Galmés, J. L. Esquivel, M. D. Velasco, A. Bastida, F. Zapata, A. Caballero and A. Frontera, *Dalton Trans.*, 2022, **51**, 1325-1332.
70. L. Zhang, Y. Zeng, X. Li and X. Zhang, *J. Mol. Model.*, 2022, **28**, 248.
71. R. Wang, Y. Lu, Z. Xu and H. Liu, *J. Phys. Chem. A*, 2021, **125**, 4173-4183.
72. S. Miao, Y. Zhang, L. Shan, M. Xu, J.-G. Wang, Y. Zhang and W. Wang, *Cryst.*, 2021, **11**, 1309.
73. Y. Xu, V. Kumar, M. J. Z. Bradshaw and D. L. Bryce, *Cryst. Growth Des.*, 2020, **20**, 7910-7920.
74. M. J. Frisch, G. W. Trucks, H. B. Schlegel, G. E. Scuseria, M. A. Robb, J. R. Cheeseman, G. Scalmani, V. Barone, G. A. Petersson, H. Nakatsuji, X. Li, M. Caricato, A. V. Marenich, J. Bloino, B. G. Janesko, R. Gomperts, B. Mennucci, H. P. Hratchian, J. V. Ortiz, A. F. Izmaylov, J. L. Sonnenberg, Williams, F. Ding, F. Lipparini, F. Egidi, J. Goings, B. Peng, A. Petrone, T. Henderson, D. Ranasinghe, V. G. Zakrzewski, J. Gao, N. Rega, G. Zheng, W. Liang, M. Hada, M. Ehara, K. Toyota, R. Fukuda, J. Hasegawa, M. Ishida, T. Nakajima, Y. Honda, O. Kitao, H. Nakai, T. Vreven, K. Throssell, J. A. Montgomery Jr., J. E. Peralta, F. Ogliaro, M. J. Bearpark, J. J. Heyd, E. N. Brothers, K. N. Kudin, V. N. Staroverov, T. A. Keith, R. Kobayashi, J. Normand, K. Raghavachari, A. P. Rendell, J. C. Burant, S. S. Iyengar, J. Tomasi, M. Cossi, J. M. Millam, M. Klene, C. Adamo, R. Cammi, J. W. Ochterski, R. L. Martin, K. Morokuma, O. Farkas, J. B. Foresman and D. J. Fox, Wallingford, CT2016.
75. Y. Zhao and D. G. Truhlar, *Theor. Chem. Acc.*, 2008, **120**, 215-241.
76. D. P. Devore, T. L. Ellington and K. L. Shuford, *J. Phys. Chem. A*, 2020, **124**, 10817-10825.
77. Q. Zhao, *J. Mol. Model.*, 2020, **26**, 329.
78. J. Yang, Q. Yu, F.-L. Yang, K. Lu, C.-X. Yan, W. Dou, L. Yang and P.-P. Zhou, *New J. Chem.*, 2020, **44**, 2328-2338.
79. B. Ren, Y. Shi, Y. Lu, Z. Xu and H. Liu, *Comput. Theor. Chem.*, 2022, **1209**, 113636.
80. S. Scheiner and S. Hunter, *ChemPhysChem.*, 2022, **23**, e202200011.
81. K. Kříž and J. Řezáč, *Phys. Chem. Chem. Phys.*, 2022, **24**, 14794-14804.
82. A. D. Boese, *ChemPhysChem.*, 2015, **16**, 978-985.
83. K. L. Schuchardt, B. T. Didier, T. Elsethagen, L. Sun, V. Gurumoorthi, J. Chase, J. Li and T. L. Windus, *J. Chem. Infor. Model.*, 2007, **47**, 1045-1052.
84. B. P. Pritchard, D. Altarawy, B. Didier, T. D. Gibson and T. L. Windus, *J. Chem. Infor. Model.*, 2019, **59**, 4814-4820.
85. S. F. Boys and F. Bernardi, *Mol. Phys.*, 1970, **19**, 553-566.
86. M. Gray, P. E. Bowling and J. M. Herbert, *J. Chem. Theory Comput.*, 2022, **18**, 6742-6756.
87. R. F. W. Bader, *Atoms in Molecules, A Quantum Theory*, Clarendon Press, Oxford, 1990.
88. S. J. Grabowski and J. M. Ugalde, *J. Phys. Chem. A*, 2010, **114**, 7223-7229.
89. M. Rozenberg, *RSC Advances*, 2014, **4**, 26928-26931.
90. T. A. Keith, TK Gristmill Software, Overland Park KS2013.

91. A. E. Reed, F. Weinhold, L. A. Curtiss and D. J. Pochatko, *J. Chem. Phys.*, 1986, **84**, 5687-5705.
92. A. E. Reed and F. Weinhold, *J. Chem. Phys.*, 1983, **78**, 4066-4073.
93. T. Lu and F. Chen, *J. Comput. Chem.*, 2012, **33**, 580-592.
94. G. Sánchez–Sanz, I. Alkorta and J. Elguero, *Molecules*, 2017, **22**, 227.
95. B. Li, X. Wang, H. Wang, Q. Song, Y. Ni, H. Wang and X. Wang, *J. Mol. Struct.*, 2022, **1265**, 133371.
96. M. Calabrese, A. Pizzi, A. Daolio, A. Frontera and G. Resnati, *Chem. Commun.*, 2022, **58**, 9274-9277.
97. V. Kumar, Y. Xu, C. Leroy and D. L. Bryce, *Phys. Chem. Chem. Phys.*, 2020, **22**, 3817-3824.

Table 1. Total and partial interaction energies (kcal/mol) and charge transfer (e)

X_1	X_3	X_4	$-E_{int}$	E_{HB}	E_{ChB}	E_{ChB}/E_{HB}	coop[a]	CT
Y=S								
NH_2	H	H	10.27	5.90	2.38	0.40	1.99	-0.026
Me	H	H	9.53	5.51	2.26	0.41	1.76	-0.025
H	H	H	9.90	6.17	2.22	0.36	1.51	-0.030
CN	H	H	12.40	9.36	2.49	0.27	0.55	-0.055
NO_2	H	H	14.31	11.54	2.75	0.24	0.02	-0.069
Me	H	O^-	17.39	16.41	4.18	0.25	3.20	-0.104
Me	NH_2	NH_2	9.52	6.51	2.53	0.39	0.48	-0.037
Me	NO_2	H	9.85	4.76	3.08	0.65	2.01	-0.004
Me	CN	CN	9.15	3.48	3.71	1.07	1.96	+0.001
Me	H	NH_3^+	11.21	4.07	7.26	1.78	0.12	+0.023
H	H	H[b]	13.67	2.76	10.00	3.62	0.91	+0.054
Y=Se								
NH_2	H	H	13.07	6.36	3.99	0.63	2.72	-0.026
Me	H	H	12.09	5.91	3.65	0.62	2.53	-0.025
H	H	H	12.39	6.62	3.45	0.52	2.32	-0.031
CN	H	H	14.95	10.24	3.37	0.33	1.34	-0.062
NO_2	H	H	17.15	12.81	3.57	0.28	0.77	-0.079
Me	H	O^-	18.69	16.37	4.28	0.26	1.96	-0.112
Me	NH_2	NH_2	12.17	6.61	3.91	0.59	1.65	-0.038
Me	NO_2	H	12.47	4.02	4.70	1.17	3.75	-0.002
Me	CN	CN	12.14	3.76	5.56	1.48	2.82	+0.064
Me	H	NH_3^+	15.51	4.11	10.21	2.48	-1.19	
H	H	H[b]	20.51	0.68	14.48	21.29	5.35	+0.098
Y=Te								
NH_2	H	H	20.28	7.71	7.74	1.00	4.83	-0.019
Me	H	H	18.56	7.05	6.79	0.96	4.72	-0.020
H	H	H	18.80	7.96	6.21	0.78	4.63	-0.029
CN	H	H	21.86	12.94	5.41	0.42	3.51	-0.077
NO_2	H	H	25.36	16.94	5.59	0.33	2.83	-0.103
Me	H	O^-	23.22	18.04	5.25	0.29	0.07	-0.124
Me	NH_2	NH_2	19.18	8.42	7.11	0.84	3.65	-0.034
Me	NO_2	H	18.79	5.57	8.27	1.48	4.95	+0.016
Me	CN	CN	19.42	4.39	9.72	2.21	5.31	+0.027
Me	H	NH_3^+	25.71	4.23	17.11	4.04	-4.37	+0.080
H	H	H[b]	32.77	1.73	23.02	13.31	8.02	+0.119

[a] $-E_{int} - E_{HB} - E_{ChB}$

[b] H^+ added to N_5 of ring

Table 2. Geometrical aspects of complexes, lengths in Å, angles in degs

X_1	X_3	X_4	R_{HB}	R_{ChB}	ΔR_{HB}[a]	ΔR_{ChB}[a]	$\Delta r(OH)$	$\Delta r(YN_5)$	$\theta(O_1H\cdot\cdot N_2)$	$\theta(N_5Y\cdot\cdot O_2)$	R_{inter}[b]
Y=S											
NH_2	H	H	1.817	2.842	0.005	-0.065	0.0200	-0.0053	170.0	177.1	4.336
Me	H	H	1.835	2.878	0.023	-0.029	0.0181	-0.0054	170.3	176.8	4.404
H	H	H	1.812	2.907	-	-	0.0222	-0.0061	169.7	176.7	4.383
CN	H	H	1.705	2.966	-0.107	0.059	0.0344	-0.0088	171.5	174.8	4.339
NO_2	H	H	1.652	2.984	-0.160	0.077	0.0443	-0.0101	170.7	174.1	4.272
Me	H	O^-	1.581	3.491	-0.231	0.584	0.0660	-0.0111	176.8	167.0	4.550
Me	NH_2	NH_2	1.785	2.924	-0.027	0.017	0.0225	-0.0051	173.1	175.5	4.412
Me	NO_2	H	1.968	2.797	0.156	-0.110	0.0094	-0.0024	160.7	175.4	4.396
Me	CN	CN	1.992	2.756	0.180	-0.151	0.0081	-0.0042	163.6	178.7	4.409
Me	H	NH_3^+	2.121	2.608	0.309	-0.299	0.0037	0.0033	159.0	180.0	4.383
H	H	H[c]	2.233	2.444	0.421	-0.463	0.0043	0.0117	151.4	178.7	4.331
Y=Se											
NH_2	H	H	1.760	2.775	0.004	-0.062	0.0259	-0.0054	169.3	170.0	4.343
Me	H	H	1.776	2.811	0.020	-0.026	0.0239	-0.0056	169.6	169.7	4.376
H	H	H	1.756	2.837	-	-	0.0285	-0.0067	169.0	169.6	4.358
CN	H	H	1.651	2.898	-0.105	0.061	0.0443	-0.0102	170.6	167.8	4.315
NO_2	H	H	1.600	2.925	-0.156	0.088	0.0568	-0.0116	169.8	167.0	4.253
Me	H	O^-	1.547	3.207	-0.209	0.370	0.0748	-0.0113	178.1	163.9	4.457
Me	NH_2	NH_2	1.734	2.830	-0.022	-0.007	0.0291	-0.0033	171.7	169.1	4.377
Me	NO_2	H	1.896	2.744	0.140	-0.093	0.0132	-0.0029	161.4	168.8	4.376
Me	CN	CN	1.909	2.694	0.153	-0.143	0.0123	-0.0014	163.9	171.5	4.377
Me	H	NH_3^+	1.976	2.517	0.220	-0.320	0.0080	0.0130	160.4	173.0	4.315
H	H	H[c]	1.949	2.305	0.193	-0.532	0.0119	0.0414	154.9	171.3	4.187
Y=Te											
NH_2	H	H	1.638	2.638	0.006	-0.066	0.0466	0.0014	168.1	160.6	4.265
Me	H	H	1.653	2.675	0.022	-0.029	0.0432	-0.0005	168.3	160.4	4.299
H	H	H	1.632	2.704	-	-	0.0503	-0.0029	167.7	160.0	4.277
CN	H	H	1.539	2.778	-0.093	0.074	0.0747	-0.0092	169.1	158.2	4.249
NO_2	H	H	1.481	2.803	-0.150	0.099	0.0973	-0.0112	168.4	157.4	4.189
Me	H	O^-	1.489	3.038	-0.143	0.334	0.0962	-0.0101	174.4	156.1	4.395
Me	NH_2	NH_2	1.615	2.678	-0.016	-0.026	0.0510	0.0072	169.7	160.0	4.291
Me	NO_2	H	1.760	2.625	0.129	-0.079	0.0255	0.0049	162.0	159.9	4.303
Me	CN	CN	1.746	2.568	0.115	-0.136	0.0274	0.0105	164.3	161.7	4.286
Me	H	NH_3^+	1.765	2.405	0.133	-0.299	0.0239	0.0516	162.5	162.9	4.222
H	H	H[c]	1.729	2.290	0.097	-0.414	0.0330	0.1608	159.9	160.5	4.147

[a]relative to $X_1=X_3=X_4=H$

[b]distance from center of ring to carboxyl C

[c]H^+ added to N_5 of ring

Table 3. NBO, E(2), AIM bond critical point density, and NMR coupling constants.[a]

X_1	X_3	X_4	E(2), kcal/mol		ρ_{BCP}, au		K, Hz	
			H··O	Y··O	H··O	Y··O	H··O	Y··O
Y=S								
NH_2	H	H	20.5	2.9	0.0396	0.0151	-2.10	32.98
Me	H	H	19.4	2.5	0.0379	0.0141	-2.19	29.90
H	H	H	21.3	2.3	0.0403	0.0133	-2.22	27.50
CN	H	H	33.8	1.8	0.0528	0.0117	-1.73	23.42
NO_2	H	H	41.5	1.7	0.0602	0.0112	-1.19	21.67
Me	H	O^-	56.4	0.3	0.0720	-	-0.15	9.24
Me	NH_2	NH_2	24.9	2.3	0.0429	0.0127	-2.15	28.75
Me	NO_2	H	9.5	3.0	0.0265	0.0163	-1.75	33.10
Me	CN	CN	8.9	3.5	0.0253	0.0179	-1.83	38.09
Me	H	NH_3^+	4.7	3.6	0.0188	0.0243	-1.53	52.56
H	H	H[b]	2.6	13.9	0.0147	0.0347	-1.24	63.67
Y=Se								
NH_2	H	H	25.8	5.1	0.0458	0.0192	-2.07	90.77
Me	H	H	24.6	4.4	0.0441	0.0179	-2.22	80.84
H	H	H	26.6	4.2	0.0465	0.0171	-2.19	75.05
CN	H	H	41.4	3.2	0.0605	0.0150	-1.35	66.47
NO_2	H	H	50.5	2.9	0.0686	0.0141	-0.58	61.06
Me	H	O^-	63.6	1.2	0.0782	0.0084	0.33	38.48
Me	NH_2	NH_2	30.4	4.4	0.0490	0.0171	-2.07	81.96
Me	NO_2	H	13.2	5.3	0.0317	0.0202	-1.96	89.10
Me	CN	CN	12.8	6.5	0.0311	0.0226	-2.09	102.25
Me	H	NH_3^+	9.2	13.5	0.0265	0.0328	-1.92	136.17
H	H	H[b]	10.2	25.6	0.0287	0.0526	-1.97	140.94
Y=Te								
NH_2	H	H	43.0	10.5	0.0623	0.0310	-1.26	189.23
Me	H	H	40.8	9.2	0.0601	0.0292	-1.57	187.34
H	H	H	44.2	8.2	0.0635	0.0278	-1.36	186.13
CN	H	H	64.3	5.9	0.0795	0.0242	0.35	180.53
NO_2	H	H	80.3	5.3	0.0916	0.0231	1.97	172.43
Me	H	O^-	79.0	2.3	0.0898	0.0156	1.60	132.74
Me	NH_2	NH_2	48.2	9.8	0.0656	0.0288	-1.14	193.15
Me	NO_2	H	24.5	10.7	0.0450	0.0317	-2.06	169.44
Me	CN	CN	26.8	13.6	0.0473	0.0357	-2.16	181.74
Me	H	NH_3^+	24.6	19.1	0.0452	0.0478	-2.25	159.24
H	H	H[b]	28.8	45.0	0.0502	0.0588	-2.05	94.21

[a]all quantities evaluated with aug-cc-pVTZ basis set. For Te, NBO and AIM utilized the all-electron aug-cc-pVTZ-DK3 for NBO and AIM, NMR-DKH(TZ2P) for K.

[b]H^+ added to N_5 of ring

Table 4. Changes in NMR chemical shielding (ppm) arising from complexation

X_1	X_3	X_4	H	O_1	N_2	O_2	Y
Y=S							
NH_2	H	H	-7.4	-4.8	61.8	11.0	-20.0
Me	H	H	-7.0	-10.8	60.7	19.3	-18.8
H	H	H	-7.4	-16.4	62.5	20.2	-17.7
CN	H	H	-9.1	-25.5	73.7	27.4	-11.8
NO_2	H	H	-10.3	-21.9	80.9	30.7	-10.5
Me	H	O^-	-12.6	-34.2	8.7	17.5	-87.3
Me	NH_2	NH_2	-7.4	-14.0	18.3	15.5	-12.5
Me	NO_2	H	-5.3	-5.9	49.6	25.5	-12.2
Me	CN	CN	-4.6	-6.1	57.3	25.9	-18.7
Me	H	NH_3^+	-3.3	-5.7	-17.6	35.7	-99.8
H	H	H[a]	-2.9	-9.3	47.9	45.3	-21.5
Y=Se							
NH_2	H	H	-8.5	-8.1	31.3	17.6	0.2
Me	H	H	-8.1	-15.7	29.3	29.0	-1.9
H	H	H	-8.5	-21.9	30.9	29.6	-8.5
CN	H	H	-10.4	-32.2	44.6	38.2	2.0
NO_2	H	H	-11.7	-28.0	54.8	38.7	5.9
Me	H	O^-	-13.4	-38.7	9.4	21.1	-129.7
Me	NH_2	NH_2	-8.3	-19.3	23.6	25.9	-7.2
Me	NO_2	H	-6.3	-10.5	18.9	35.9	-4.1
Me	CN	CN	-5.8	-10.7	21.4	37.1	5.9
Me	H	NH_3^+	-4.8	-10.8	-7.2	51.6	-75.7
H	H	H[a]	-5.6	-20.2	24.6	71.4	86.1
Y=Te							
NH_2	H	H	-11.4	-19.6	53.4	35.0	331.6
Me	H	H	-10.8	-31.4	48.6	55.1	296.2
H	H	H	-11.3	-39.2	48.8	54.6	267.4
CN	H	H	-13.3	-51.7	64.0	64.0	217.5
NO_2	H	H	-15.1	-46.4	80.6	58.0	216.7
Me	H	O^-	-14.8	-49.9	32.8	34.2	81.1
Me	NH_2	NH_2	-10.9	-36.2	33.1	53.6	343.6
Me	NO_2	H	-8.6	-24.4	34.2	62.8	354.4
Me	CN	CN	-8.7	-26.4	41.8	67.3	352.6
Me	H	NH_3^+	-8.3	-29.1	54.3	93.8	546.3
H	H	H[a]	-9.6	-46.2	69.8	122.8	872.2

[a]H^+ added to N_5 of ring

Table 5. Extrema in molecular electrostatic potential (kcal/mol) occurring on isolated monomers[a]

X_1COOH	max	min
X_1		
NH_2	50.9	-38.8
Me	50.9	-34.6
H	55.5	-31.7
CN	71.6	-21.3
NO_2	78.4	-24.3[b]
ring X_3,X_4	Y=S	
H,O^-	-79.1	-104.6
H,H	13.7	-25.7
NH_2,NH_2	5.8	-28.2
NO_2,H	28.6	-26.4
CN,CN	37.2	-8.7
H,H,H^+	127.1	+67.5
H,NH_3^+	97.8	+50.0
	Y=Se	
H,O^-	-72.8	-103.6
H,H	20.0	-26.4
NH_2,NH_2	13.1	-28.6
NO_2,H	34.0	-27.9
CN,CN	43.9	-10.2
H,H,H^+	136.0	+64.5
H,NH_3^+	105.7	+48.6
	Y=Te	
H,O^-	-61.5	-102.8
H,H	32.6	-28.2
NH_2,NH_2	27.4	-30.1
NO_2,H	35.9	-28.0
CN,CN	57.1	-13.3
H,H,H^+	153.5	+59.9
H,NH_3^+	121.1	+45.9

[a]located on 0.001 au isodensity surface

[b]on other side of O from incoming Y

Table 6. Correlation coefficients for linear relationship with E_{HB} and E_{ChB}

	all		S		Se		Te	
	HB	ChB	HB	ChB	HB	ChB	HB	ChB
$\Delta r(OH)/\Delta r(YN_2)$	0.84	0.80	0.98	0.75	0.95	0.94	0.94	0.92
E(2)	0.99	0.89	0.96	0.68	0.96	0.95	0.94	0.91
ρ_{BCP}	0.98	0.87	0.91	0.94	0.94	0.91	0.93	0.93
K	0.60	0.33	0.46	0.62	0.78	0.71	0.95	0.50
$\Delta\sigma(H)$	0.73		0.89		0.92		0.89	
$\Delta\sigma(O_1)$	0.41		0.84		0.64		0.35	
$\Delta\sigma(N_2)$	0.02		0.00		0.08		0.01	
$\Delta\sigma(O_2)$		0.82		0.66		0.78		0.83
$\Delta\sigma(Y)$		0.58		0.19		0.95		0.92
$V_{max}*V_{min}$	0.63	0.48	0.64	0.41	0.66	0.54	0.65	0.67

Table 7. Thermodynamic quantities for complexation reaction at 25 C.

X_1	X_3	X_4	ΔH, kcal/mol	ΔS, cal/mol K	ΔG, kcal/mol
Y=S					
NH_2	H	H	-8.86	-33.07	1.00
Me	H	H	-8.23	-33.36	1.72
H	H	H	-8.54	-33.74	1.52
CN	H	H	-10.69	-34.60	-0.38
NO_2	H	H	-12.21	-35.25	-1.70
Me	NH_2	NH_2	-8.21	-33.46	1.76
Me	H	O^-	-14.05	-31.35	-4.71
Me	NO_2	H	-8.58	-34.04	1.57
Me	CN	CN	-7.93	-33.60	2.08
Me	H	NH_3^+	-10.04	-33.64	-0.01
H	H	H^b	-11.98	-33.54	-1.98
Y=Se					
NH_2	H	H	-11.48	-35.29	-0.96
Me	H	H	-10.62	-35.30	-0.10
H	H	H	-10.86	-35.54	-0.26
CN	H	H	-12.95	-35.77	-2.29
NO_2	H	H	-14.52	-36.34	-3.68
Me	H	O^-	-14.99	-33.93	-4.87
Me	NH_2	NH_2	-10.66	-35.39	-0.11
Me	NO_2	H	-11.10	-35.36	-0.55
Me	CN	CN	-10.84	-34.91	-0.43
Me	H	NH_3^+	-13.96	-35.98	-3.23
H	H	H^b	-17.39	-37.36	-6.25
Y=Te					
NH_2	H	H	-17.05	-38.95	-5.44
Me	H	H	-15.75	-37.67	-4.52
H	H	H	-15.80	-37.89	-4.51
CN	H	H	-17.66	-38.11	-6.30
NO_2	H	H	-19.41	-38.18	-8.03
Me	H	O^-	-17.67	-36.23	-6.86
Me	NH_2	NH_2	-15.97	-37.31	-4.85
Me	NO_2	H	-16.32	-37.88	-5.02
Me	CN	CN	-16.83	-37.39	-5.68
Me	H	NH_3^+	-22.19	-37.80	-10.92
H	H	H^b	-27.00	-39.97	-15.08

[b]H^+ added to N_5 of ring

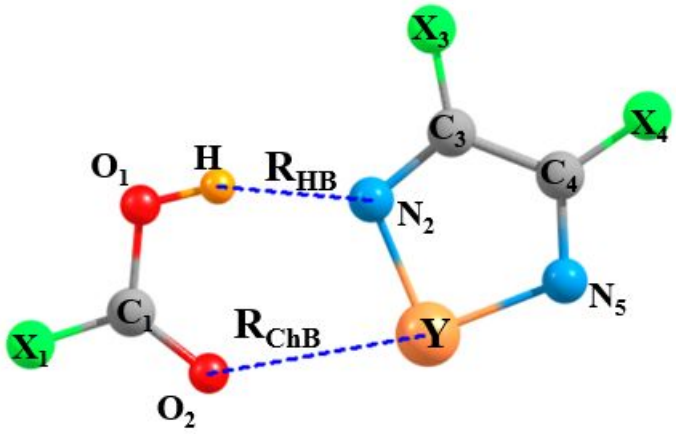

Fig 1. Schematic diagram of complexes showing atomic labeling.

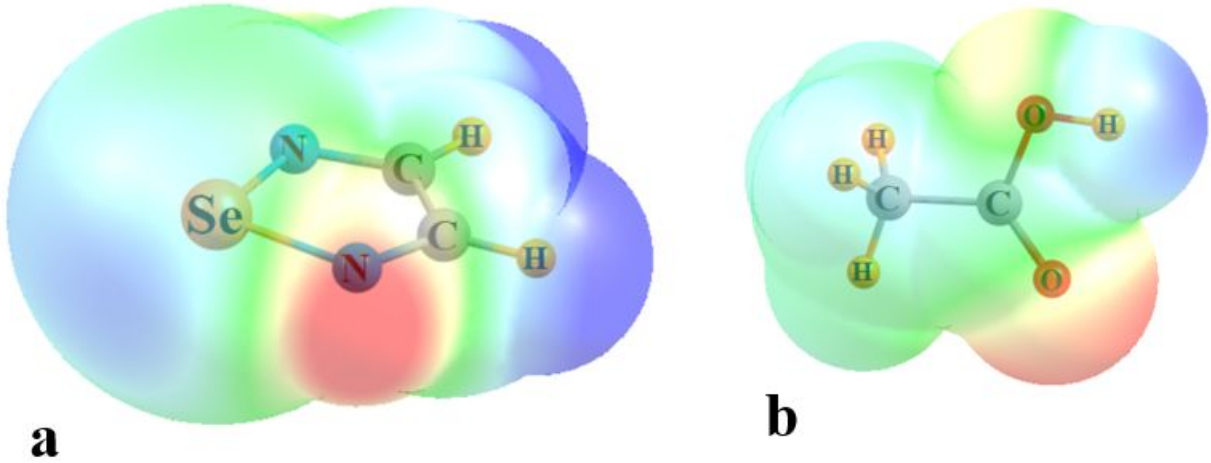

Fig 2. Molecular electrostatic potential on a surface 1.5 x vdW atomic radii surrounding a) selenadiazole where blue and red indicate respectively +19 and -31 kcal/mol and b) MeCOOH where blue and red refer to ±44 kcal/mol.